nature cell biology

Intraflagellar transport is required for polarized recycling of the TCR/CD3 complex to the immune synapse

Francesca Finetti[1], Silvia Rossi Paccani[1], Maria Giovanna Riparbelli[1], Emiliana Giacomello[2], Giuseppe Perinetti[3], Gregory J. Pazour[4], Joel L. Rosenbaum[5] and Cosima T. Baldari[1,6]

Most eukaryotic cells have a primary cilium which functions as a sensory organelle[1]. Cilia are assembled by intraflagellar transport (IFT), a process mediated by multimeric IFT particles and molecular motors[2]. Here we show that lymphoid and myeloid cells, which lack primary cilia, express IFT proteins. IFT20, an IFT component essential for ciliary assembly[3,4], was found to colocalize with both the microtubule organizing centre (MTOC) and Golgi and post-Golgi compartments in T-lymphocytes. In antigen-specific conjugates, IFT20 translocated to the immune synapse. *IFT20* knockdown resulted in impaired T-cell receptor/CD3 (TCR/CD3) clustering and signalling at the immune synapse, due to defective polarized recycling. Moreover, IFT20 was required for the inducible assembly of a complex with other IFT components (IFT57 and IFT88) and the TCR. The results identify IFT20 as a new regulator of immune synapse assembly in T cells and provide the first evidence to implicate IFT in membrane trafficking in cells lacking primary cilia, thereby introducing a new perspective on IFT function beyond its role in ciliogenesis.

When naive T cells encounter antigen-presenting cells (APCs) bearing cognate major histocompatibility complex (MHC)-bound peptide antigen, a dynamic rearrangement of membrane and cytosolic molecules occurs at the T-cell–APC contact area. This results in the formation of a highly organized interface known as the immune synapse, which functions as a platform for signal integration, fine-tuning and extinction[5,6]. A hallmark of the nascent immune synapse is reorientation of the MTOC towards the APC[7], which ensures targeted delivery of signalling molecules from intracellular pools to the immune synapse[8]. This includes delivery of the TCR/CD3 complex, which is carried to the immune synapse through polarized recycling[9]. Directional movement of structural and regulatory molecules, orchestrated by the MTOC, is a characteristic feature of primary cilia. These projections, present on most non-dividing cells, function as sensory organelles, relaying information from the external environment into the cell through IFT, a process carried out by multimeric IFT particles and molecular motors[2,10].

Unlike most other eukaryotic cell types, hematopoietic cells lack primary cilia[10]. Surprisingly, IFT20, an IFT component essential for ciliary assembly[3,4], was found to be expressed in human cells of both lymphoid (peripheral blood lymphocytes and Jurkat T-lymphoma cells) and myeloid (monocytes and monocyte-derived dendritic cells) lineages (Fig. 1a). Similar results were obtained in mouse, where IFT20 was detectable in central (thymus and bone marrow) and peripheral (lymph node and spleen) lymphoid organs (Fig. 1a). Immunofluorescence analysis of Jurkat cells and human peripheral blood lymphocytes showed that IFT20 was localized to a discrete cytosolic region centered around the MTOC (Fig. 1b for Jurkat cells; Supplementary Information, Fig. S1a for human peripheral blood lymphocytes), which duplicated at early prophase (data not shown). No IFT20 staining was detectable during metaphase and anaphase, with the exception of two small punctate structures corresponding to the MTOCs (Fig. 1b–d), as confirmed by co-staining with anti-γ-tubulin antibodies (Fig. 1c, d), and by the IFT20 staining pattern in cells extracted with Triton X-100 to solubilize cell membranes (Supplementary Information, Fig. S1b). At late telophase and cytokinesis, IFT20 reassembled in the larger structure surrounding the MTOC (Fig. 1b). Excluding the staining corresponding to the MTOC(s) (~40% colocalization), the pattern of IFT20 localization was indicative of the Golgi, which undergoes fragmentation during mitosis. Co-staining of Jurkat cells with antibodies specific to Golgi markers or other membrane compartments showed that IFT20 colocalizes to a significant extent (~60%) with the cis-Golgi (identified by GM130; Fig. 1c, d). Treatment of Jurkat cells with brefeldin-A, which induces Golgi fragmentation, resulted in a largely similar dissipation of Golgi- and IFT20-specific immunostaining (Supplementary Information, Fig. S1c), further supporting the Golgi association of IFT20. It was found that IFT20 also colocalized, albeit to a more limited extent, with the trans-Golgi network (identified by TGN46; ~23%), recycling endosomes (identified by TfR; ~19%) and early endosomes (identified by EEA1; ~16%), whereas minimal colocalization with lysosomes (identified by LAMP-1; < 10%) was detected (Fig. 1c, d). Hence, IFT20 is expressed in T-lymphocytes where it colocalizes with both the Golgi and MTOC,

[1]Department of Evolutionary Biology and [2]Department of Neuroscience, University of Siena, Via Aldo Moro 2, 53100 Siena, Italy. [3]Department of Biomedicine, University of Trieste, 34138 Trieste, Italy.; [4]Program in Molecular Medicine, University of Massachussetts Medical School, Worcester, MA 01605, USA. [5]Department of Molecular, Cellular and Developmental Biology, Yale University, New Haven, CT 06520, USA.
[6]Correspondence should be addressed to C.T.B.(e-mail: baldari@unisi.it).

Received 10 July 2009; accepted 18 August 2009; published online 25 October 2009; DOI: 10.1038/ncb1977

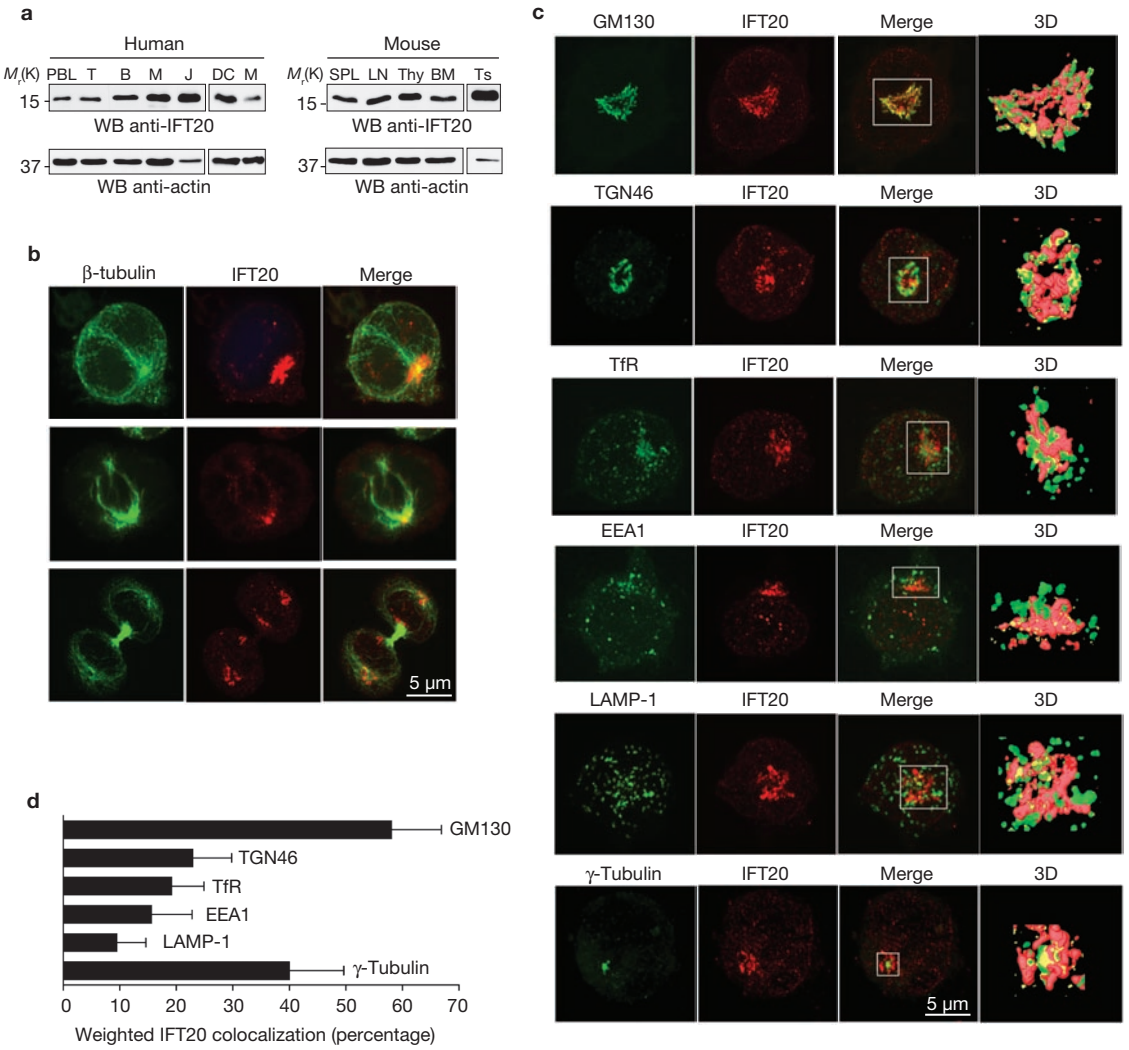

Figure 1 IFT20 is expressed in T-cells and associates with the Golgi apparatus and MTOC. (**a**) Immunoblot analysis of IFT20 in lysates of human and murine lymphoid and myeloid cells. PBL, peripheral blood lymphocytes; T, T cells; B, B cells; M, monocytes; J, Jurkat cells; DC, dendritic cells; SPL, spleen; LN, lymph node; Thy, thymus; BM, bone marrow; Ts, testis (positive control). (**b**, **c**) Immunofluorescence analysis of IFT20 localization in Jurkat cells co-stained with antibodies against β-tubulin (**b**) or γ-tubulin (**c**) or markers of membrane compartments. (**b**) Cells are shown in interphase (top), metaphase (middle) and telophase (bottom). (**c**) Images show *z*-stack projections. The white boxes in the merges represent the field of views for the 3D reconstructions (right panels) that are based on sequential 0.5-μm sections. The corresponding animations are shown in the supplementary information, Movies 1–6. GM130, cis-Golgi; TGN46, trans-Golgi network; TfR, recycling endosomes; EEA1, early endosomes; LAMP-1, lysosomes. (**d**) Quantification of the weighted colocalization (percentage) of the different subcellular organelles/compartments with IFT20 staining (mean ± s.d., 30 cells were analysed for each marker). All of the pairwise comparisons of IFT20 colocalizations with GM130, TGN46, TfR, EEA1, LAMP-1 and γ-tubulin were statistically significant ($P < 0.01$) with only two exceptions, TGN46 versus TfR and TfR versus EEA1.

as it does in ciliated cells[10], notwithstanding the absence of a primary cilium. Moreover, IFT20 associates, albeit to a lesser extent, with other membrane compartments implicated in protein trafficking.

Among the most dramatic events in immune synapse formation is the translocation of the MTOC and Golgi to the contact area between T cells and APCs[7]. As IFT20 associates with both organelles, we analysed the localization of IFT20 in conjugates of Jurkat T cells and Raji B cells (used as APCs) loaded with staphyloccal enterotoxin E (SEE). IFT20 was found to translocate to the immune synapse, together with the MTOC and Golgi, in T cells (Fig. 2a, b; Supplementary Information, Fig. S2a). As expected, the TCR/CD3 complex clustered at the immune synapse, concomitant with MTOC and Golgi reorientation (Fig. 2a, b). Similar effects occurred after capping the TCR/CD3 complex using anti-CD3 mAb and secondary antibodies (Supplementary Information, Fig. S2b), a procedure which results in TCR/CD3 clustering and MTOC and Golgi reorientation under the TCR cap[11]. IFT20 translocation to the immune synapse in antigen-specific conjugates was also observed in T-cells purified from healthy donors (Fig. 2f). Interestingly, IFT20 not only clustered at the immune synapse together with the TCR, but also inducibly associated with the receptor complex subunits CD3ζ and CD3ε in response to TCR engagement (Fig. 2c). No association with the linker for activation of T-cells (LAT), which also localizes at the immune synapse, was detected (data not shown), underscoring the specificity of the IFT20–CD3 interaction.

To assess the potential role of IFT20 in immune synapse formation, *IFT20* expression was stably knocked down in Jurkat cells by

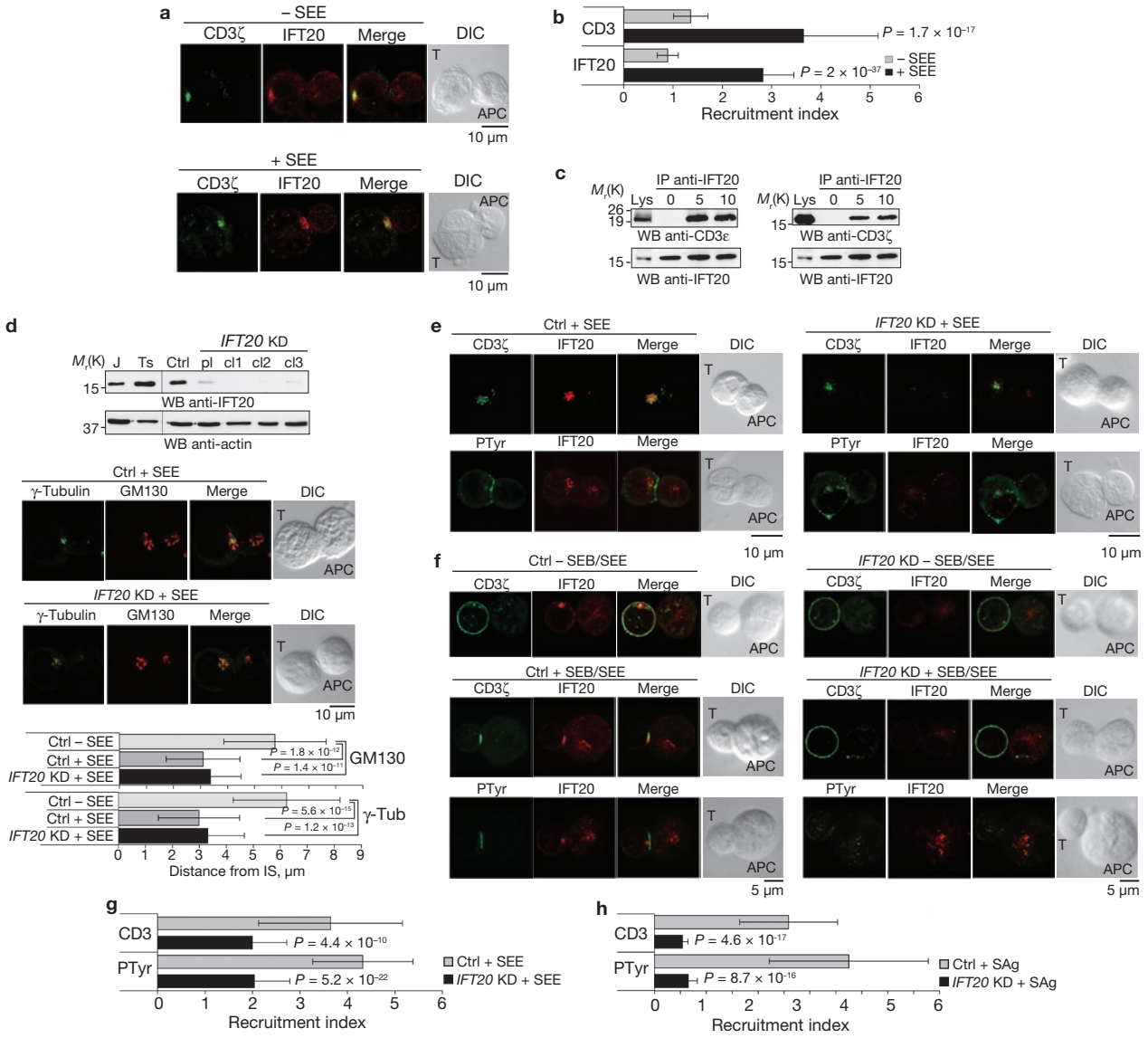

Figure 2 IFT20 is required for TCR/CD3 clustering and signalling at the immune synapse. (**a**) Immunofluorescence analysis of IFT20 and CD3ζ localization in conjugates of Jurkat cells and APCs, in the presence (+) or absence (–) of SEE. Median optical sections are shown. (**b**) IFT20 and CD3ζ fluorescence at the T-cell–APC contact site relative to that at the remaining T-cell membrane (CD3ζ) or T-cell area (IFT20), expressed as relative recruitment index. Measurements on conjugates from ≥ 3 independent experiments ($n = 50$ conjugates). Error bars are mean ± s.d. (**c**) Immunoblotting with anti-CD3ζ and anti-CD3ε antibodies of IFT20-specific immunoprecipitates from lysates of Jurkat cells either unstimulated or stimulated with anti-CD3 mAb for 5–10 min (for full scan of blot see Supplementary Information Fig. S6a). (**d**) Top panel, immunoblot of IFT20 in lysates of Jurkat cells (J), a Jurkat line transfected with empty vector (Ctr), and three Jurkat clones (cl1–3) transfected with constructs encoding *IFT20*-specific siRNA (*IFT20* KD; for full scan of blot see Supplementary Information Fig. S6b; all samples were run on the same gel). A pool (pl) of the three *IFT20*-knockdown clones (IFT20 reduction in the pool ~75%) was used for subsequent experiments. Ts, positive control. Bottom panel, Mean distance ± s.d. of the MTOC and of the central point of the cis-Golgi from the T-cell–APC contact site (immune synapse, IS). Measurements on conjugates from ≥ 3 independent experiments ($n = 50$ conjugates). Middle panels, immunofluorescence analysis of SEE-specific conjugates of control or *IFT20*-knockdown Jurkat cells and APCs. Cells were co-stained with anti-γ-tubulin and anti-GM130 antibodies. (**e**, **f**) Immunofluorescence analysis of SEE-specific conjugates of control or *IFT20*-knockdown Jurkat cells and APCs (**e**) or of SEB/SEE-specific conjugates using peripheral T-cells transiently transfected with empty vector or the *IFT20* RNAi construct (IFT20 reduction ~40%, ~80% and ~70% for donors 1–3, respectively, as assessed by immunoblotting) (**f**). Cells were co-stained with anti-IFT20 and either anti-CD3ζ or anti- PTyr antibodies. (**g**, **h**) CD3ζ or PTyr fluorescence at the T-cell–APC contact site relative to that at the remaining T-cell membrane (CD3ζ) or T-cell area (PTyr), expressed as relative recruitment index, in Jurkat cells (**g**) and T cells from healthy donors (**h**). Measurements on conjugates from ≥ 3 independent experiments for Jurkat cells ($n = 50$ conjugates), or on conjugates from duplicate samples from three independent donors for peripheral T-cells ($n = 30$ conjugates, 10 per donor). DIC, differential interference contrast. T, T-cell. KD, knockdown. Ctrl, control.

RNA interference (RNAi; Fig. 2d). A transfectant generated with an empty vector was used as a control. Both the MTOC and Golgi translocated to the immune synapse in *IFT20*-knockdown cells stimulated with SEE-loaded APCs, similarly to control cells (Fig. 2d). However, CD3ζ immunostaining revealed that clustering of the TCR/CD3 complex at the immune synapse was impaired in these cells (Fig. 2e, g). Moreover, the number of conjugates with TCR/CD3 clustering at the immune synapse was significantly reduced (*IFT20*-knockdown cells

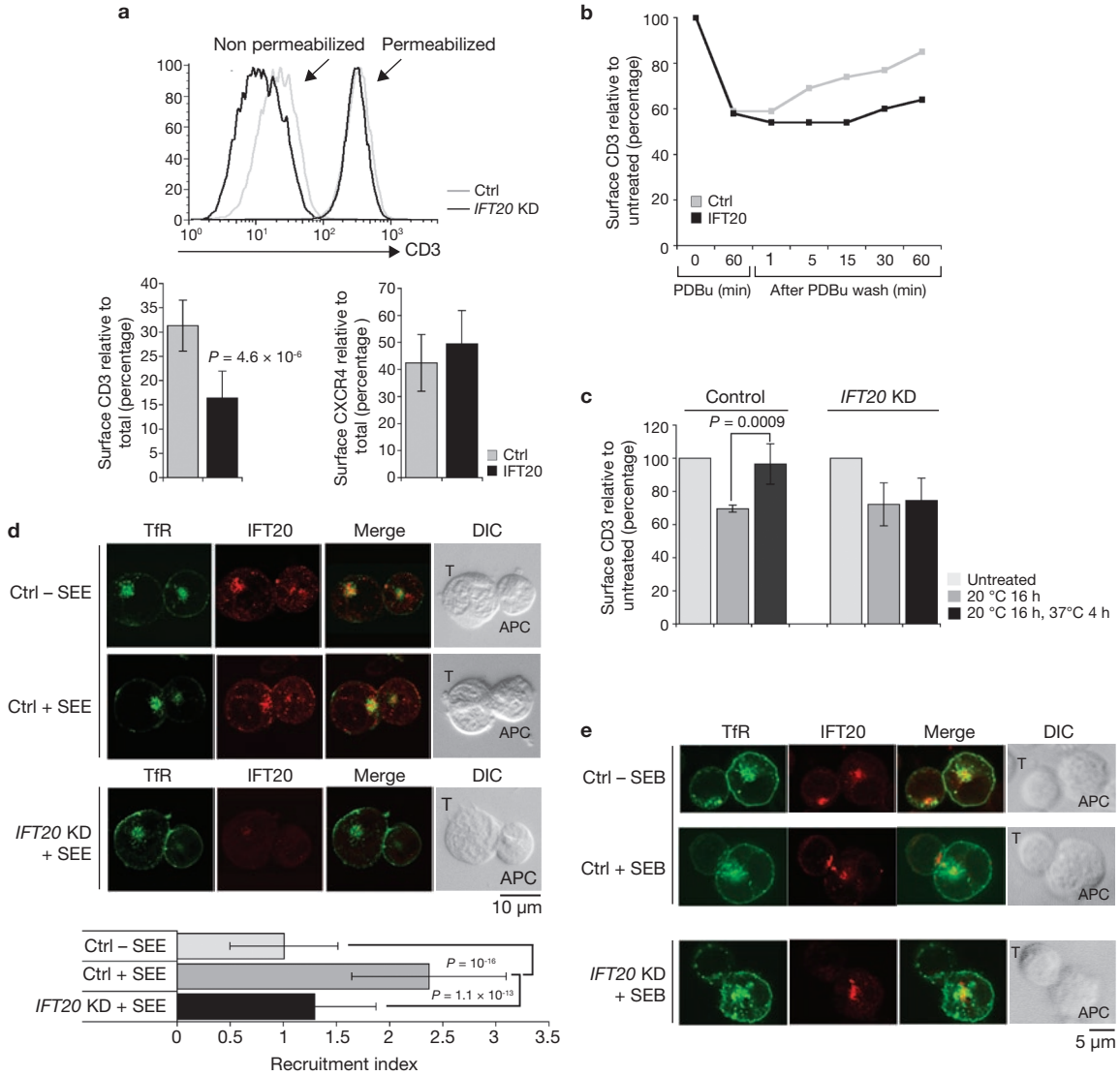

Figure 3 IFT20 is required for trafficking of the TCR/CD3 complex in recycling endosomes. (**a**) Representative FACS profiles and plots showing levels of CD3 in intact (surface CD3) relative to permeabilized (total CD3) control ($n = 9$) and *IFT20*-knockdown ($n = 14$) Jurkat cells. Data from similar experiments are shown for CXCR4 (right; $n = 5$ for control and 6 for *IFT20*-knockdown cells). (**b**) Relative levels of surface CD3 in control/*IFT20*-knockdown cells untreated, treated with PDBu for 1 h or treated with PDBu and then washed and incubated at 37 °C for the indicated times. A representative experiment is shown ($n = 4$). (**c**) Relative levels of surface CD3 in control/*IFT20*-knockdown cells untreated, or incubated at 20 °C for 16 h, or incubated at 20 °C then shifted to 37 °C for 4 h. Receptor expression was measured by flow cytometry, and calculated from the mean fluorescence intensity (MFI) levels ($n = 3$ experiments). Surface CD3 recovery was 88.8% in control versus 8.3% in *IFT20*-knockdown cells ($P = 0.019$). (**d**) Immunofluorescence analysis of IFT20 and recycling endosome (TfR) localization in conjugates of control or *IFT20*-knockdown Jurkat cells and APCs, either unpulsed or pulsed with SEE. Median optical sections are shown. The graph (bottom) shows TfR fluorescence at the T cell–APC contact site relative to that at the remaining T-cell area (expressed as relative recruitment index). $n = 50$ conjugates for control, no SEE (4 experiments); $n = 54$ conjugates for control with SEE (4 experiments), $n = 54$ conjugates for *IFT20*-knockdown with SEE (3 experiments). (**e**) Immunofluorescence analysis, with anti-TfR and anti-IFT20 antibodies, of TfR localization in SEB-specific conjugates using SEB-specific peripheral T cells from a representative healthy donor transiently transfected with either an empty vector or a *IFT20* RNAi construct ($n = 3$ donors). Error bars in **a**, **c** and **d** represent mean ± s.d. KD, knockdown. Ctrl, control.

41%, $n = 128$ versus control cells 70%, $n = 111$). Similar results were obtained when CD3ε was immunostained (Supplementary information, Fig.S3a). A comparable pattern was observed when T-cells were co-incubated for longer times with antigen-loaded APCs (data not shown), ruling out a delay in TCR clustering at the immune synapse. Consistent with these findings, TCR/CD3 cross-linking resulted in impaired receptor capping (Supplementary Information, Fig. S2b). A defect in TCR/CD3 clustering at the immune synapse in antigen-specific conjugates was also observed in T-cells purified from healthy donors and transiently knocked down for *IFT20* expression (Fig. 2f, h; Supplementary Information, Fig. S3d, e).

Clustering at the immune synapse is required to bring the TCR close to the tyrosine kinase Lck, which phosphorylates conserved motifs in the intracellular domains of the CD3 complex. These motifs recruit the tyrosine kinase ZAP-70, which becomes activated and phosphorylates key protein substrates to initiate TCR signalling[12]. To assess the outcome of *IFT20* knockdown on signalling by the TCR at the immune synapse, SEE-specific conjugates were immunostained with

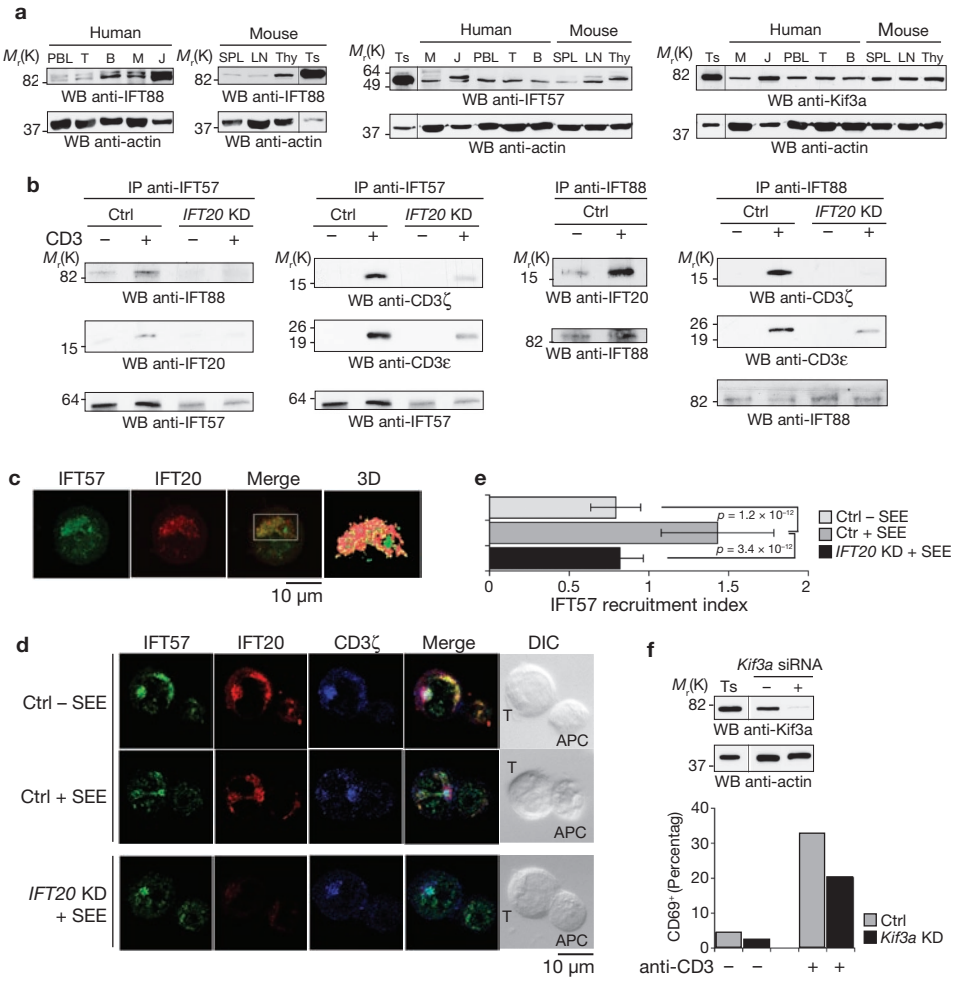

Figure 4 IFT20 inducibly associates with other IFT components in response to TCR activation. (**a**) Immunoblotting analysis of IFT88, IFT57 and Kif3a in human and murine lymphoid and myeloid cell lysates (samples were run on the same gel). PBL, peripheral blood lymphocytes; T, T-cells; B, B cells; M, monocytes; J, Jurkat cells; SPL, spleen; LN, lymph node; Thy, thymus; BM, bone marrow; Ts, testis (positive control). (**b**) Immunoblotting analysis, with the indicated antibodies, of anti-IFT57- or anti-IFT88-specific immunoprecipitates from lysates of Jurkat cells either unstimulated or stimulated with anti-CD3 mAb for 10 min (for full scans of blots see Supplementary Information Fig. S6c, d). A mouse testis lysate was included in each gel as control (data not shown). (**c**) Immunofluorescence analysis of IFT57 and IFT20 localization in Jurkat cells. A *z*-stack projection is shown (3D). The white box in the merge represents the field of view for the 3D reconstruction based on sequential 0.5-μm sections. The corresponding animation is shown in Supplementary Information, Movie 7. Weighted colocalization (as percentage) with the IFT20 staining was 42.0 ± 7.4 ($n = 30$ cells). (**d**) Immunofluorescence analysis of IFT57 and IFT20 localization in conjugates of control or *IFT20*-knockdown Jurkat cells and APCs, in the presence or absence of antigen (SEE). Cells were co-stained with antibodies against CD3ζ. Median optical sections are shown. (**e**) IFT57 fluorescence at the T cell–APC contact site relative to that at the remaining T-cell area (expressed as relative recruitment index). Error bars represent mean ± s.d. Measurements were taken from 30 conjugates for each condition. (**f**) Percentages of $CD69^+$ control or *Kif3a*-knockdown Jurkat cells after stimulation by CD3 cross-linking for 8 h, as assessed by flow cytometric analysis of surface CD69. The values of duplicate samples from one representative experiment out of three are shown. An anti-Kif3a immunoblot of lysates of control and Kif3a-knockdown Jurkat cells is shown (samples were run on the same gel).

anti-phospho-tyrosine antibodies. Compared with control cells, where strong and localized staining at the immune synapse was observed in a large proportion of conjugates (75%, $n = 139$), a small proportion of *IFT20*-knockdown Jurkat cells (38%, $n = 161$) contained phosphotyrosine staining at the immune synapse. Staining was, moreover, significantly different, appearing to be weaker and dispersed throughout the cell (Fig. 2e, g). Similar results were obtained from peripheral T-cells transiently knocked down for *IFT20* expression (Fig. 2f, h; Supplementary Information, Fig. S3e). As tyrosine kinase activation occurs at the cell surface in response to TCR engagement, the data suggest a rapid dissociation of phosphorylated proteins from the immune synapse. Consistent with this finding, both the extent and duration of tyrosine phosphorylation was reduced in *IFT20*-knockdown cells, as assessed by immunoblotting analysis of cell lysates (Supplementary Information, Fig. S3b). Moreover, signalling was not productive, as shown by defective upregulation of the surface activation marker CD69 in response to TCR engagement in *IFT20*-knockdown cells (Supplementary Information, Fig. S3c).

Clustering of the TCR/CD3 complex at the immune synapse is achieved through a combination of lateral diffusion, cytoskeleton-driven movement and polarized recycling[5]. The IFT20 association with both Golgi and post-Golgi compartments suggests a potential role of IFT20 in intracellular trafficking of the TCR/CD3 complex. To investigate this, the proportion of cellular CD3 detectable at the cell surface was measured by flow cytometric analysis of intact and permeabilized cells. Although the total levels of CD3 were similar in control and *IFT20*-knockdown

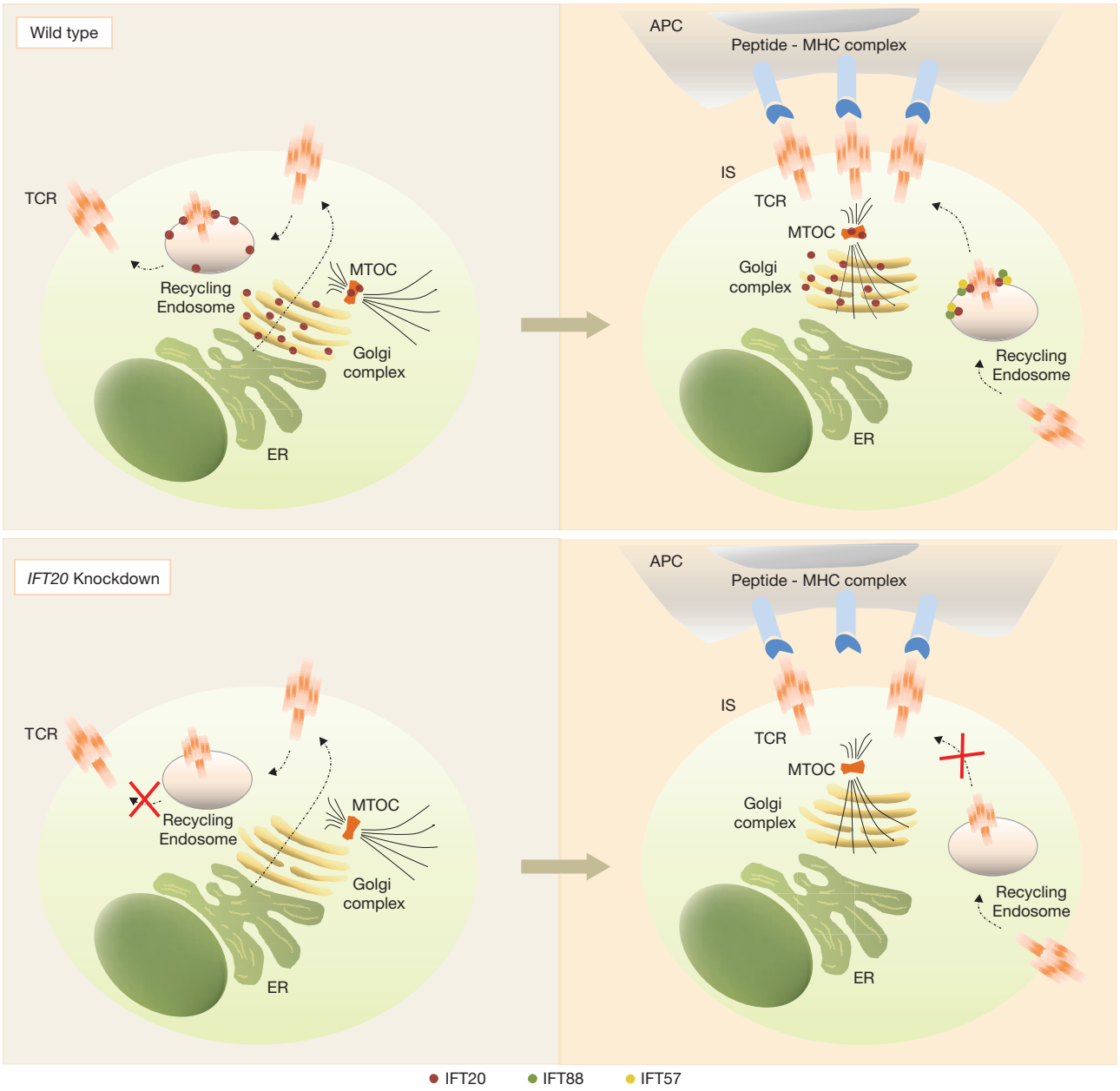

Figure 5 Schematic representation of the localization and function of IFT20 in TCR/CD3 trafficking and immune synapse formation. Top, in resting T-cells, IFT20, which is associated with the Golgi complex, the microtubule-organizing centre (MTOC) and recycling endosomes, regulates constitutive T-cell antigen receptor (TCR) recycling to the cell surface (left). When the TCR is engaged by cognate peptide antigen presented by MHC on the surface of an antigen-presenting cell (APC), IFT20 promotes TCR clustering at the immune synapse (IS) through polarized recycling, as a complex with IFT57 and IFT88. Bottom, in the absence of IFT20, both constitutive TCR recycling (left) and polarized TCR recycling to the immune synapse (right) are impaired. Conversely, translocation of the Golgi and MTOC to the immune synapse is not affected by the absence of IFT20. ER, endoplasmic reticulum.

cells, less surface CD3 was expressed in *IFT20*-knockdown cells than in control cells, resulting in a lower ratio of surface CD3 to total CD3 in *IFT20*-knockdown cells (Fig. 3a; Supplementary Information, Fig. S4a). Conversely, no alteration in the ratio of surface to total receptor was observed either for the chemokine receptor CXCR4 (Fig.3a) or for CD69 (data not shown). These data suggest a role of IFT20 in membrane trafficking of the TCR/CD3 complex.

Assembly of the TCR/CD3 complex is initiated in the endoplasmic reticulum and completed in the Golgi, from where it moves to the cell surface via the canonical exocytic route. Once exposed, the TCR/CD3 complex undergoes several rounds through the constitutive recycling pathway, which involves a di-leucine motif in the CD3γ cytosolic tail, before being targeted for degradation[13]. The rates of both *de novo* synthesis and constitutive endocytosis leading to degradation are very low, indicating that, in resting cells, surface TCR expression is principally dependent on TCR recycling[13,14]. To investigate the potential role of IFT20 in this process, we capitalized on the capacity of phorbol esters to activate a pathway that depends on PKC (protein kinase C)-mediated

activation of the CD3γ di-leucine motif and leads to TCR recycling[13]. Control and *IFT20*-knockdown cells were treated with PDBu (phorbol 12,13-dibutyrate) for 1 h, which resulted in ~40% TCR internalization. The time course of surface CD3 recovery after PDBu removal was monitored by flow cytometry. In contrast with control cells, which readily recovered surface CD3, no increase in surface CD3 was detected in *IFT20*-knockdown cells (Fig. 3b), suggesting that, whereas IFT20 is dispensable for internalization of the TCR/CD3 complex, it is required for TCR/CD3 recycling back to the cell surface. To address this point further, control and *IFT20*-knockdown cells were incubated for 16 h at 20 °C to block trafficking through constitutively recycling endosomes (which resulted in ~40% reduction of surface CD3) and were then shifted to 37 °C for 4 h. The 37 °C shift resulted in recovery of surface CD3 in control, but not in *IFT20*-knockdown, cells (Fig. 3c). No changes in total CD3 were observed after either the 20 °C block or the 37 °C shift (Supplementary Information, Fig. S4b). Ligand-dependent TCR endocytosis, while activating an alternative pathway which leads to receptor degradation in lysosomes[13], was also not affected by *IFT20* knockdown, as measured in a time course analysis of TCR internalization (Supplementary Information, Fig. S4c), further ruling out endocytosis defects. Collectively, these data support the notion that IFT20 controls TCR/CD3 exocytosis through the constitutive recycling pathway. Recycling endosomes have been demonstrated to polarize to the immune synapse, thereby providing a means of TCR/CD3 enrichment at this location[9]. Notably, as opposed to control cells, recycling endosomes failed to polarize to the immune synapse, both in *IFT20*-knockdown Jurkat cells (Fig. 3d; Supplementary Information, Fig. S5) and in peripheral T-cells transiently knocked down for *IFT20* expression (Fig. 3e), indicating that IFT20 is required for polarized TCR/CD3 recycling.

In primary cilia IFT20 is a subunit of complex B, one of the two multiprotein complexes forming the IFT particle[1,2]. To understand whether IFT20 interacts with other IFT components in the absence of primary cilia, T cells were tested by immunoblotting for expression of other complex-B components. Both human and murine cells were found to express IFT88 and IFT57, as well as the kinesin Kif3a, the motor powering anterograde IFT (Fig. 4a). Co-immunoprecipitation experiments revealed the existence of an IFT20–IFT88–IFT57 complex, which was enhanced in response to TCR engagement (Fig. 4b). Similarly to IFT20, IFT88 and IFT57 inducibly interacted with the TCR/CD3 complex in response to stimulation (Fig. 4b). Moreover, immunofluorescence analysis showed that IFT57, which was found to colocalize to a significant extent with IFT20 in resting cells (Fig. 4c), clustered with the TCR and IFT20 at the immune synapse (Fig. 4d). Remarkably, both the association of IFT88 with IFT57 and their interaction with the TCR/CD3 complex were impaired in *IFT20*-knockdown cells (Fig. 4b). Furthermore, IFT57 was not recruited to the immune synapse in *IFT20*-knockdown cells (Fig. 4d, e). Notably, similar to the results obtained from *IFT20*-knockdown cells, transient knockdown of *Kif3a* by RNAi resulted in defective antigen-specific conjugate formation (73.4% of control cells, $n = 79$ versus 50.3% of *Kif3a*-knockdown cells, $n = 145$) and impaired T-cell activation, as shown by the reduction in TCR-dependent CD69 expression (Fig. 4f). Taken together, these data indicate that IFT20 drives the assembly of IFT-like particles in T-lymphocytes in response to TCR engagement, and they support the notion that IFT20 functions together with other IFT components in immune synapse formation and T-cell activation.

T-cell commitment to activation requires sustained TCR signalling[15]. MTOC-driven polarization of recycling endosome-localized TCR/CD3 complexes to the to the immune synapse represents an important means of mobilizing fresh supplies of receptor to this location as engaged receptors are internalized and targeted to lysosomes for degradation[9]. Our data show that IFT20 contributes to the formation of a functional immune synapse by regulating TCR/CD3 recycling (Fig. 5). The inducible association of IFT20, IFT88 and IFT57 with the TCR/CD3 complex suggests that, in response to a signal triggered by surface TCRs, initially clustered at the immune synapse through lateral diffusion and F-actin-dependent movement[5], IFT20, in concert with IFT88 and IFT57, may assist in delivering recycling endosome-localized TCR/CD3 to the immune synapse while the MTOC polarizes towards the contact site with the APC.

Based on the structural similarities of IFT components with COPI (coat protein complex I) proteins[16], which are involved in exocytosis and endosome function[17], it has been hypothesized that IFT evolved as a specialized form of coated vesicle transport. In this model, coated vesicle transport from the Golgi defined a new plasma membrane domain, which then evolved to become the modern cilium[16]. This idea is supported by the finding that, in ciliated cells, IFT20 is not only localized to cilia and the peri-basal body region, like the other IFT polypeptides, but is also linked to the Golgi through the golgin GMAP210 (refs 3, 18), suggesting that it may function as an adaptin in coupling to the IFT particle vesicles containing membranous protein cargo destined for the cilium. Our data strengthen this hypothesis by providing the first evidence that in cells lacking cilia, such as T-lymphocytes, an IFT-like particle (whose assembly is driven by IFT20 in response to extracellular cues) is integrated in the membrane trafficking pathways to orchestrate central processes, such as signalling at the immune synapse. In these cells, the membrane patch at the immune synapse, with the underlying MTOC, would represent the functional homologue of the primary cilium. This specialized membrane patch would transiently and inducibly assemble to coordinate the rapid movement of specific membranous cargo — the TCR/CD3 complex — towards the contact site with the APC. A major general implication of these data is that IFT proteins may participate in intracellular membrane trafficking in all eukaryotic cells in addition to their well established roles in ciliary assembly. In this respect, the association of defects in IFT motors and particles with human diseases such as polycystic kidney disease, *situs inversus* and retinal degeneration[19], which have been attributed to impaired ciliogenesis, may need to be revised in the wider context of intracellular protein trafficking.

METHODS

Methods and any associated references are available in the online version of the paper at http://www.nature.com/naturecellbiology/.

Note: Supplementary Information is available on the Nature Cell Biology website.

ACKNOWLEDGEMENTS

The authors want to thank G. Callaini for invaluable help with fluorescence microscopy, S. Grassini for technical assistance, A. Alcover, S. Valitutti, P. Lupetti, A. Luini, A. Colanzi, A. De Matteis and C. Mencarelli for useful discussions and J. L Telford and A. Alcover for critical reading of the manuscript. This work was supported by grants from AIRC (to C.T.B.) and the National Institutes of Health (GM060992 to G.J.P. and GM-14,642 to J.L.R.). F.F. is the recipient of a FIRC fellowship.

AUTHOR CONTRIBUTIONS

F.F., S.R.P., C.T.B., G.J.P. and J.L.R. planned the project and drafted the manuscript; F.F., S.R.P., M.G.R. and E.G. carried out the experimental work; F.F., S.R.P., C.T.B., E.G., G.P. and M.G.R. analysed the data.

COMPETING FINANCIAL INTERESTS

The authors declare no competing financial interests.

Published online at http://www.nature.com/naturecellbiology/
Reprints and permissions information is available online at http://npg.nature.com/reprintsandpermissions/

1. Scholey, J. M. & Anderson, K. V. Intraflagellar transport and cilium-based signaling. *Cell* **125,** 439–442 (2006).
2. Rosenbaum, J. L. & Witman, G. B. Intraflagellar transport. *Nature Rev. Mol. Cell Biol.* **3,** 813–825 (2002).
3. Follit, J. A., Tuft, R. A., Fogarty K. E. & Pazour, G. J. The intraflagellar transport protein IFT20 is associated with the Golgi complex and is required for cilia assembly. *Mol. Biol. Cell* **17,** 3781–3792 (2006).
4. Jonassen, J. A., San Agustin, J., Follit, J. A. & Pazour, G. J. Deletion of IFT20 in the mouse kidney causes misorientation of the mitotic spindle and cystic kidney disease. *J. Cell Biol.* **183,** 377–384 (2008).
5. Cemerski, S. & Shaw, A. Immune synapses in T-cell activation *Curr. Opin. Immunol.* **18,** 298–304 (2006).
6. Dustin, M. L., Tseng, S. Y., Varma, R. & Campi, G. T cell-dendritic cell immunological synapses. *Curr. Opin. Immunol.* **18,** 512–516 (2006).
7. Sancho, D. *et al.* Regulation of microtubule-organizing center orientation and actomyosin cytoskeleton rearrangement during immune interactions. *Immunol. Rev.* **189,** 84–97 (2002).
8. Martin-Cofreres, N. B. *et al.*, MTOC translocation modulates IS formation and controls sustained T cell signaling. *J. Cell Biol.* **182,** 951–962 (2008).
9. Das, V. *et al.*, Activation-induced polarized recycling targets T cell antigen receptors to the immunological synapse; involvement of SNARE complexes. *Immunity* **20,** 577–588 (2004).
10. Pazour, G. J. & Witman, G. B. The vertebrate primary cilium is a sensory organelle. *Curr. Opin. Cell Biol.* **15,** 105–110 (2003).
11. Wulfing, C. *et al.*, Interface accumulation of receptor/ligand couples in lymphocyte activation: methods, mechanisms, and significance. *Immunol. Rev.* **189,** 64–83 (2002).
12. Kane, L. P., Lin, J. & Weiss, A. Signal transduction by the TCR for antigen. *Curr. Opin. Immunol.* **12,** 242–249 (2000).
13. Geisler, C. TCR trafficking in resting and stimulated T cells. *Crit. Rev. Immunol.* **24,** 67–86 (2004).
14. Alcover, A. & Alarcon, B. Internalization and intracellular fate of TCR-CD3 complexes. *Crit. Rev. Immunol.* **20,** 325–346 (2000).
15. Lanzavecchia, A. & Sallusto, F. From synapses to immunological memory: the role of sustained T cell stimulation. *Curr. Opin. Immunol.* **12,** 92–98 (2000).
16. Satir, P., Mitchell, D. R. & Jekely, G. How did the cilium evolve? *Curr. Top. Dev. Biol.* **85,** 63–82 (2008).
17. Bethune, J., Wieland, F. & Moelleken, J. COPI-mediated transport. *J. Membr. Biol.* **211,** 65–79 (2006).
18. Follit, J. A. *et al.* The Golgin GMAP210/TRIP11 anchors IFT20 to the Golgi complex. *PLoS Genet.* **4**, e1000315 (2008).
19. Pazour, G. J. & Rosenbaum, J. L. Intraflagellar transport and cilia-dependent diseases. *Trends Cell Biol.* **12,** 551–555 (2002).

METHODS

Cells, plasmids, antibodies and reagents. Cell lines included Jurkat T cells and Raji B cells, both of human origin. Stable *IFT20*-knockdown Jurkat transfectants were generated as described previously[20] using two pGP676.13 plasmid constructs containing the complementary oligonucleotides corresponding to the coding region of human *IFT20* (ref. 3). Human *Kif3a*-specific siRNAs (5′-GCCUAAAGGAAGCUACAAA-3′ and 5′-UUUGUAGCUUCCUUUA-GGC-3′, Sigma-Aldrich) were transfected by electroporation and assays carried out after 72 h.

Human peripheral blood mononuclear cells (PBMCs) were purified from whole blood by density gradient centrifugation on Ficoll-Paque (Amersham Pharmacia Italia srl) and subsequently depleted of monocytes by adherence. T and B cells were purified from monocyte-depleted PBMCs, by negative or positive selection, respectively, by immunomagnetic sorting using anti-CD19 antibody-conjugated beads (Dynal Biotech). Cells were then checked for purity (which was consistently > 90%) by flow cytometry with fluorochrome-conjugated anti-CD3/anti-CD19 mAbs. Peripheral T-cells, purified with the StemSep Human T-cell enrichment kit (Voden medical Instruments SpA), were transfected with the same plasmids used for Jurkat cells using the Amaxa nucleofector device (Amaxa Biosystems) and the conditions for T-cell transfection recommended by the manufacturer. Cells were analysed 24 h and 48 h post-transfection. For the TfR labelling experiments, SEB-specific T-cells were expanded before transfection as described previously[9]. Dendritic cells were derived from peripheral blood monocytes from healthy donors as described previously[21]. Mouse cells were derived from 129sv mice (Charles River Italia). Mice were killed by cervical dislocation and thymus, lymph nodes, spleen, bone marrow and testis were collected. Single-cell suspensions were prepared using cell strainer filters (BD Falcon; BD Biosciences Europe). Bone marrow was obtained from femurs by flushing with RPMI supplemented with 7.5% fetal calf serum, and single-cell suspensions were prepared by gentle pipetting. Animal experiments were performed in agreement with the Guiding Principles for Research Involving Animals and Human Beings and approved by the local ethics committees. Polyclonal anti-IFT20, -IFT57 and -IFT88 antibodies were previously described[22]. Anti-TfR mAb (hybridoma OKT9) was provided by A. Alcover (Institut Pasteur, Paris, France). Anti-CXCR4 antibodies were provided by J. Hoxie (University of Pennsylvania, PA, USA), Leukosite and the MRC AIDS Reagent Project. IgG from OKT3 (anti-CD3; American Type Culture Collection) hybridoma supernatants were purified using Mabtrap (Amersham Biosciences Inc.) and titrated by flow cytometry. Anti-Kif3a antibodies were from Sigma-Aldrich; anti-phosphotyrosine and anti-LAT antibodies from Upstate Biotechnology Inc.; anti-CD3ε, anti-CD3ζ mAb from Santa Cruz Biotechnology; anti-LAMP-1 mAb from Developmental Studies Hybridoma Bank; anti-actin mAb from Chemicon International Inc.; anti-GM130 and anti-EEA1 mAb from BD Biosciences; anti-γ-tubulin from Sigma; anti-β-tubulin from Boehringer; anti-TGN46 from AbD Serotec. Unlabelled secondary antibodies were from Cappel (ICN Pharmaceuticals Inc), and secondary peroxidase-labelled antibodies from Amersham Pharmacia Biotech. Alexa Fluor 488- and 555-labelled secondary antibodies were from Molecular Probes (Invitrogen srl), FITC-conjugated anti-mouse Ig from DAKO (Glostrup). FITC or PE-labelled anti-human CD69, CD3 and CD19 were purchased from BD Biosciences.

Staphylococcal enterotoxin B (SEB) and E (SEE) was purchased from Toxin Technology, Cell Tracker Blue from Molecular Probes, poly-L-lysine, phorbol 12,13-dibutyrate (PDBu) and Brefeldin-A from Sigma.

Golgi extraction. For the Golgi extraction, Jurkat cells were plated on polylysine-coated wells of diagnostic microscope slides (Erie Scientific Company), where they were allowed to adhere for 15 min. After adhesion, cells were pre-extracted with PBS containing 0.1% Triton X-100 for 30 s and fixed for 10 min in methanol at –20 °C. Alternatively, cells were treated with 10 μg ml^{-1} Brefeldin A for 30 min at 37 °C and, after washing, frozen on microscope slides and fixed in cold methanol.

Activations, immunoprecipitations and immunoblotting. Activation by TCR/CD3 cross-linking was performed by incubating Jurkat cells with saturating concentrations of anti-CD3 mAb and 50 μg ml^{-1} secondary antibodies for 1–10 min at 37 °C as described previously[23]. Cells (1×10^6 per sample for direct immunoblotting analysis, 5×10^7 per sample for immunoprecipitations) were lysed in 1% Triton X-100 in 20 mM Tris-HCl (pH 8) and 150 mM NaCl in the presence of a protease inhibitor cocktail, and postnuclear supernatants were probed as such or immunoprecipitated using anti-IFT20, -IFT88 or -IFT57 polyclonal antibodies and protein A-Sepharose (Amersham). Immunoblotting was carried out using primary antibodies and peroxidase-labelled secondary antibodies, according to the manufacturer's instructions and a chemiluminescence detection kit (Pierce Rockford.). All blots were reprobed with loading (anti-actin mAb) or immunoprecipitation (anti-IFT20, -IFT57, -IFT88) control antibodies after stripping. Blots were scanned using a laser densitometer (Duoscan T2500; Agfa) and quantified using the ImageQuant 5.0 software (Molecular Dynamics).

For analysis of CD69 expression, cells (1×10^6 cells per sample) were activated by CD3 cross-linking on secondary antibody-coated plates as described previously[23] and were processed for flow cytometry 8 h after activation.

Flow cytometry. CD3, CD69 or CXCR4 expression on Jurkat transfectants and purified peripheral T-cells was quantified by flow cytometry using fluorochrome-labelled mAb (CD3, CD69) or unlabelled antibody (CXCR4) followed by FITC-labelled secondary antibodies. To analyse total expression of CD3, CD69 and CXCR4, cells were fixed in 4% paraformaldehyde in PBS for 20 min, incubated in PBS 1% BSA for 20 min, permeabilized with PBS 0.1% Triton X-100 and labelled as above.

CD3 recycling was induced by treatment with PDBu. Control and *IFT20*-knockdown Jurkat cells (1×10^6 cells ml^{-1} RPMI1640 supplemented with 10% serum) were stimulated with 1 μM PDBu for 1 h at 37 °C, washed at 4 °C and transferred to 37 °C for 1–60 min. Surface CD3 expression was measured at all time points by flow cytometry.

To block endosome recycling, control and *IFT20*-knockdown Jurkat cells were incubated at 20 °C for 16 h (1×10^6 cells ml^{-1} RPMI1640 supplemented with 10% serum). Cells were subsequently washed and transferred to 37 °C for 4 h. Surface and total CD3 expression was measured by flow cytometry as described above. TCR internalization was quantified as described previously[24,25]. Flow cytometry was carried out using a FACScan flow cytometer (Becton Dickinson). Data were acquired using CellQuest and analysed and plotted using Flowjo (TreeStar).

Immunofluorescence microscopy. Jurkat cells or PBL (1.5×10^5 cells per 4μl PBS) were plated on microscope slides, flash-frozen on a copper bar pre-cooled in liquid nitrogen and fixed by immersion in methanol for 10 min at -20 °C. For the immune synapse experiments, Raji cells (used as APCs) were pulsed for 2 h with 10 μg ml^{-1} SEE and labelled with 10 μM Cell Tracker Blue for the last 20 min. APCs were washed, mixed with Jurkat cells (1:1) for 15 min and plated on polylysine-coated wells of diagnostic microscope slides (Erie Scientific Company). Alternatively, peripheral T-cells purified from healthy donors and transiently transfected with either empty vector or the *IFT20* RNAi construct were mixed with SEE/SEB-pulsed APCs and processed as above. Cells were allowed to adhere for 15 min and then fixed in methanol at -20 °C for 10 min, as described above. Antigen-independent conjugates were obtained by mixing T-cells and APCs in the absence of SEE/SEB. To induce capping, Jurkat cells were incubated for 30 min with anti-CD3ε mAb at 4 °C and, after washing, incubated at 37 °C with secondary Alexa Fluor 488-conjugated secondary antibodies for 10 min. Cells were then washed, flash-frozen and fixed as described above.

Following fixation, samples were washed for 5 min in PBS and incubated with primary antibodies overnight at 4 °C or 1 h at room temperature. After washing in PBS, samples were incubated for 1 h at room temperature with Alexa Fluor 488- and 555-labelled secondary antibodies. For the triple staining experiment, the anti-IFT20 antibody was labelled with a Zenon Rabbit IgG Labeling Kit (Molecular Probes), using Alexa Fluor-546 as fluorochrome, and IFT57 and CD3ζ were stained with Alexa Fluor-488 and -647 labelled secondary antibodies, respectively. To better visualize surface CD3 and surface TfR, which are partially lost in methanol-fixed cells, in one experiment SEE-specific conjugates were also fixed in 4% paraformaldehyde and stained with anti-CD3ε or anti-TfR mAb (Supplementary Information, Figs S3a and S5a, b).

Confocal microscopy was carried out on a Zeiss LSM510 using a 63X objective. Z series of optical sections were performed at 0.5-μm increments. Images to quantify were acquired with pinholes opened to obtain optical sections of 0.6-μm. Detectors were set to detect an optimal signal below the saturation limits. Image sets to be compared were acquired during the same session and using the same acquisition settings. Images were processed with LSM5 Image Examiner software (Carl Zeiss).

Epifluorescence microscopy was carried out using an Axio Imager Z1 (Carl Zeiss) microscope equipped with a HBO 50-W mercury lamp for epifluorescence and

DOI: 10.1038/ncb1977

with an AxioCam HR cooled charge-coupled camera (Carl Zeiss). Grey-scale digital images were collected separately and then pseudo-coloured and merged using Adobe Photoshop 7.0 software (Adobe Systems). If required, images were adjusted for contrast in Adobe Photoshop. When comparisons were to be made between images, the photos were taken in identical conditions and manipulated equally.

Post-processing of confocal images, colocalization analyses and 3D reconstructions. Clustering or relocalization of molecules and organelles at the T cell–APC contact site was quantified on median optical confocal sections using ImageJ software (downloaded from http://www.embl-heidelberg.de/eamnet/) and expressed either as relative recruitment index (IFT20, CD3ζ, PTyr, TfR) or as distance of the centre of the organelle from the T cell–APC contact site (MTOC, Golgi), as described previously[9,26].

Post-processing of the confocal images included an initial segmentation by a semi-automatic intensity-independent zero-crossing procedure, which allowed the identification of the boundaries of the organelles/compartments[27]. Specifically, colocalization analysis and 3D reconstructions were performed on the images segmented by an edge-detection intensity-independent zero-crossing procedure. In this procedure, the edges of the structural elements are assumed to correspond to the inflection points of the intensity functions. At these positions, the absolute values of the slope are maximal, and therefore the first derivative shows a maximum, and the Laplacian (the second derivative) changes sign, that is, crosses zero[28]. These zero-crossings have thus been used as the tool for the recognition of edges/surfaces in 2D/3D microscopy imaging[27]. Briefly, all of the images were slightly pre-smoothed with a Gaussian filter ($\sigma = 2$) to reduce noise and the background pixels below 15% of the maximum point spread function intensity were cut before calculating the zero-crossing algorithm, which was run through a dedicated MATLAB (The Mathworks Inc., R2006b) routine. The same MATLAB routine was used to calculate the weighted colocalizations (see below). Finally, the DIPimage software (version 1.6, http://www.diplib.org/), was used to develop the 3D reconstructions readable in the Visual Molecular Dynamics package (version 1.8.5, http://www.ks.uiuc.edu/Research/vmd/), which was used to visualize these 3D reconstructions.

Object-based weighted colocalizations of each of the examined organelles/compartments with the IFT20 staining, and the corresponding 3D reconstructions, were elaborated from the segmented images as described previously[27]. First, after the zero-crossing segmentation has been performed, only the remaining pixels for each channel are taken into account. Second, these pixels are subdivided into three regions: all the pixels where only channel 1 (IFT20) is present belong to region 1, all the pixels where only channel 2 (any other marker) is present belong to region 2. Finally, all pixels where both channels are present belong to region 3. For the weighted colocalization of any of the cellular compartment/organelle (region 2) with IFT20 (region 1), the ratio between the intensity of pixels in region 3 to the intensities of pixels in region 2+3 was calculated.

Statistical analyses. Microsoft Excel was used for data analysis. Quantitative data are shown as mean ± s.d. Moreover, after testing for the normality of the data by means of a Shapiro-Wilk test and the equality of variance among the datasets by means of a Levene test, parametric methods were used to assess the significance of the differences among the treatments/groups (data from at least three independent experiments). A one-way analysis of variance (ANOVA) was used in every comparison involving more than two treatments/groups. Thereafter, a Bonferroni-corrected Student's *t*-test for unpaired samples was used in the pairwise comparisons. $P < 0.05$ was considered statistically significant.

20. Pacini, S. *et al.*,Tyrosine 474 of ZAP-70 is required for association with the Shc adaptor and for T-cell antigen receptor-dependent gene activation. *J. Biol. Chem.* **273,** 20487–20493 (1998).
21. Sallusto, F., Cella, M., Danieli, C. & Lanzavecchia, A. Dendritic cells use macropinocytosis and the mannose receptor to concentrate macromolecules in the major histocompatibility complex class II compartment: downregulation by cytokines and bacterial products. *J. Exp. Med.* **182,** 389–400 (1995).
22. Pazour, G. J. *et al.* The intraflagellar transport protein, IFT88, is essential for vertebrate photoreceptor assembly and maintenance. *J. Cell Biol.* **157,** 103–113 (2002).
23. Boncristiano, M. *et al.,* The Helicobacter pylori vacuolating toxin inhibits T cell activation by two independent mechanisms. *J. Exp. Med.* **198,** 1887–1897 (2003).
24. D'Oro, U. *et al.* Regulation of constitutive TCR internalization by the zeta-chain. *J. Immunol.* **169,** 6269–6278 (2002).
25. Patrussi, L. *et al.* Cooperation and selectivity of the two Grb2 binding sites of p52Shc in T-cell antigen receptor signaling to Ras family GTPases and Myc-dependent survival. Oncogene **24,** 2218–2228 (2005).
26. Esquerré, M. *et al.* Human regulatory T cells inhibit polarization of T helper cells toward antigen-presenting cells via a TGF-beta-dependent mechanism. *Proc. Natl Acad. Sci. USA* **105,** 2550–2555 (2008).
27. Perinetti, G. *et al.* Correlation of 4Pi and electron microscopy to study transport through single Golgi stacks in living cells with super resolution. *Traffic* **10,** 379–391 (2009).
28. O'Haver, T. C. Potential clinical applications of derivative and wavelength-modulation spectrometry. *Clin. Chem.* **25,** 1548–1553 (1979).

nature cell biology

DOI: 10.1038/ncb1977

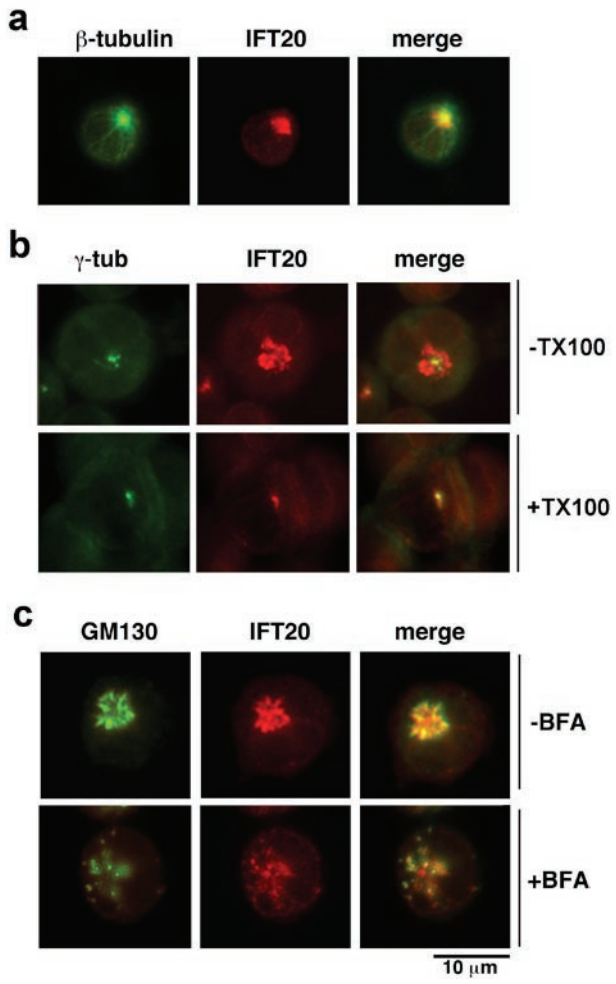

Figure S1 a. Immunofluorescence analysis of IFT20 localization in PBL costained with anti-β-tubulin antibodies. **b**. Immunofluorescence analysis of IFT20 localization in Jurkat cells, either untreated or subjected to Triton X-100 extraction. Cells were costained with anti-γ-tubulin antibodies. **c**. Immunofluorescence analysis of IFT20 localization in Jurkat cells costained with antibodies against the cis-Golgi marker GM130. Cells were either untreated (top) or treated with Brefeldin-A (BFA).

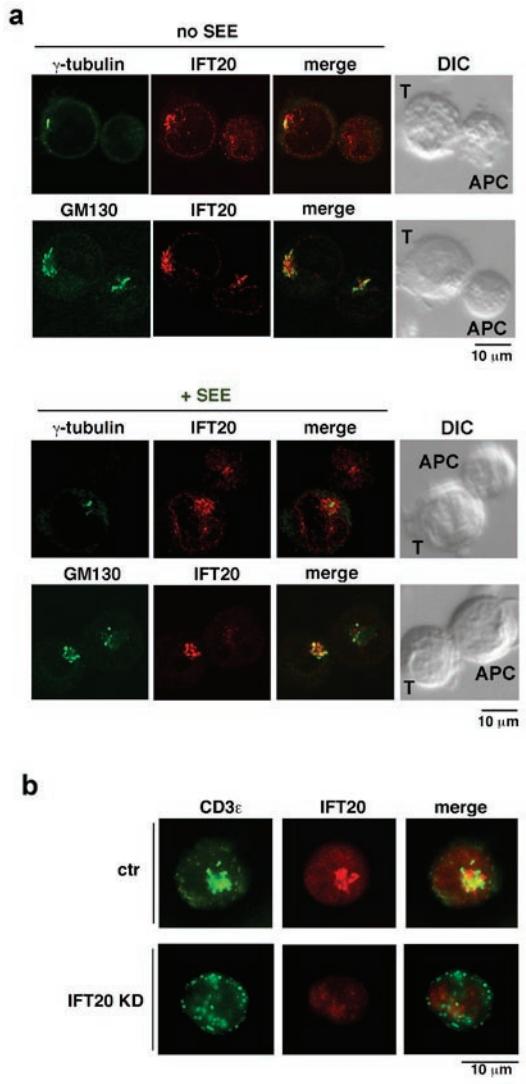

Figure S2 a. Immunofluorescence analysis of IFT20 localization in conjugates of Jurkat cells and APC, in the presence or absence of SEE. Cells were costained with antibodies against γ-tubulin, GM130 or CD3ζ. Before conjugate formation, APC were stained with Cell Tracker Blue for identification. Median optical sections are shown. **b**. Immunofluorescence analysis of IFT20 localization in control (top) or IFT20-KD (bottom) Jurkat cells costained with antibodies against CD3ε. Cells were incubated with anti-CD3 mAb and secondary antibody for 15 min at 37°C to induce capping.

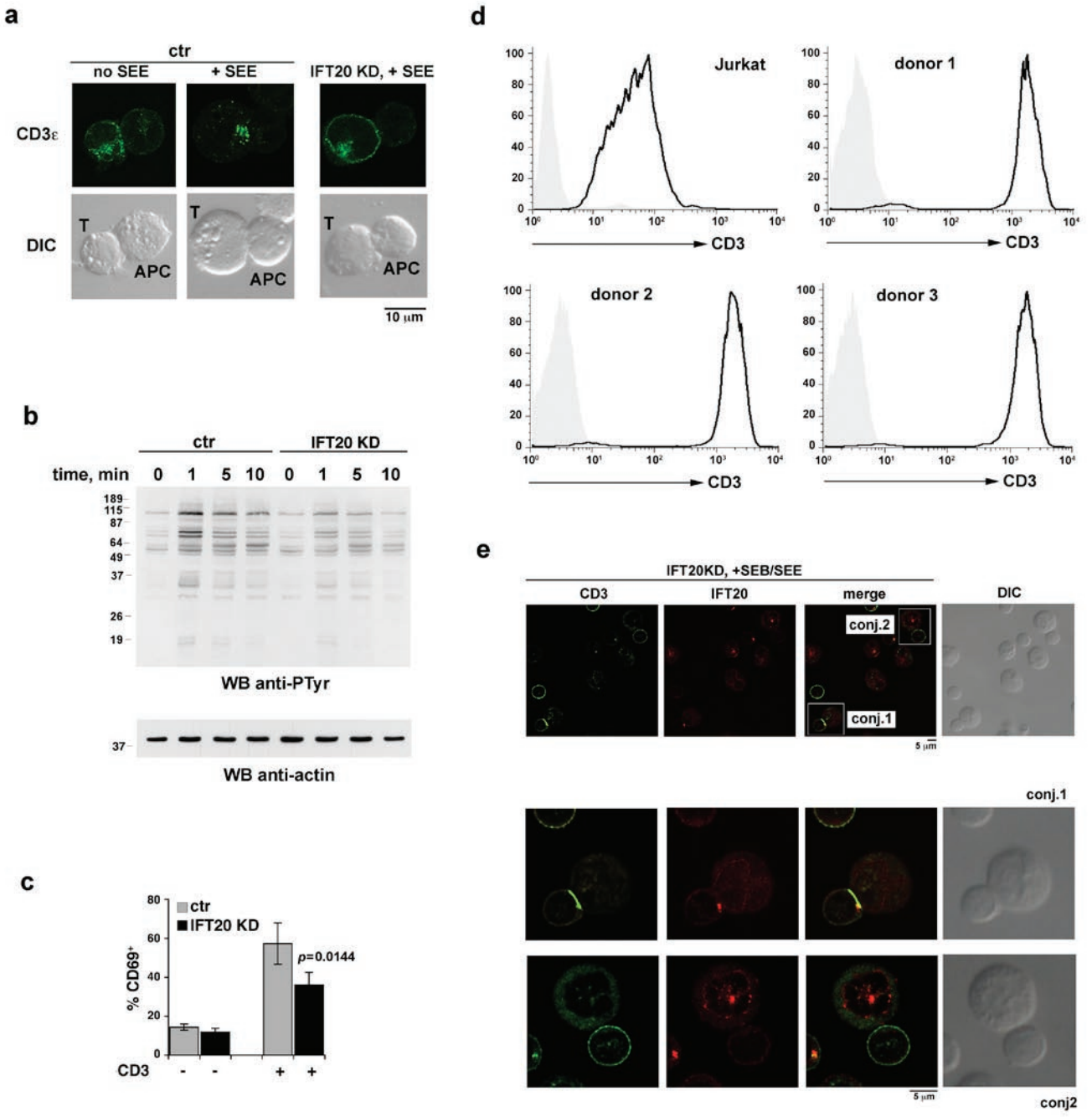

Figure S3 a. Immunofluorescence analysis of CD3ε localization in conjugates of control/IFT20-KD Jurkat cells and APC, in the presence or absence of SEE. Before conjugate formation, Raji cells were stained with CTB (blue) for identification. Cells were fixed in non-permeabilizing conditions. Median confocal sections are shown. **b**. Anti-phosphotyrosine immunoblot of lysates of control or IFT20-KD Jurkat cells either unstimulated or stimulated with anti-CD3 mAb for the indicated times. A control anti-actin blot is shown below. The migration of molecular mass markers is indicated. **c**. Percentages of $CD69^+$ control or IFT20-KD Jurkat cells following stimulation by CD3 cross-linking for 8h, as assessed by flow cytometric analysis of surface CD69 (n=4). Error bars, SD. **d**. Flow cytometric analysis of surface TCR/CD3 expression on Jurkat cells and on T cells purified from peripheral blood from 3 independent healthy donors. Note the significantly higher TCR expression on peripheral T-cells compared to Jurkat cells, which accounts for the better immunostaining. **e**. Immunofluorescence analysis with anti-CD3ζ and anti-IFT20 antibodies of SEB/SEE-specific conjugates using purified peripheral T cells transiently transfected with either empty vector or the IFT20 RNAi construct. No CD3ζ clustering can be observed in conjugate 2, where IFT20 was effectively knocked down, as opposed to conjugate 1, which still expresses IFT20, and where CD3ζ and IFT20 cluster at the IS. A low magnification field, where the 2 conjugates are highlighted, is shown in the top row.

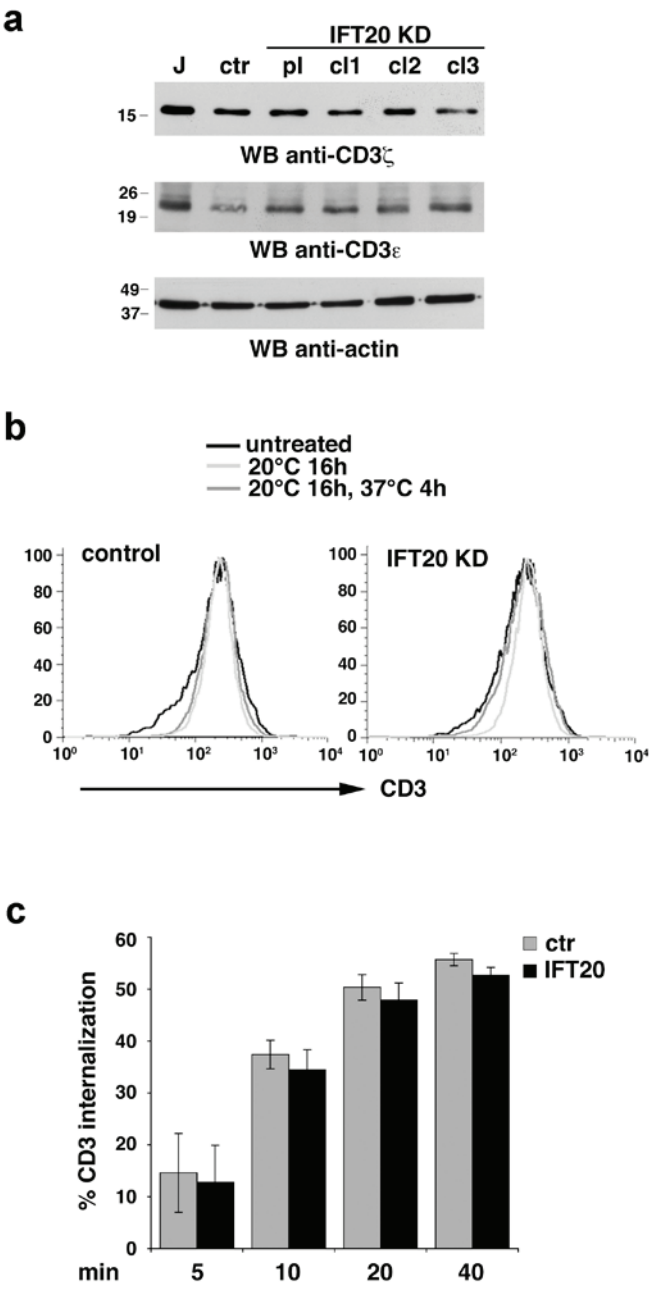

Figure S4 a. Immunoblot analysis of CD3ζ and CD3ε expression in lysates of parental Jurkat cells, a Jurkat line stably transfected with empty vector (ctr), and three Jurkat clones stably transfected with constructs encoding IFT20-specific siRNA (KD). The filter was reprobed with control anti-actin antibodies. **b**. Flow cytometric analysis of CD3 in permeabilized control (top) or IFT20-KD (bottom) Jurkat cells, either untreated, or incubated for 16h at 20°C, or incubated for 16h at 20°C then shifted to 37°C for 4h. Representative profiles are shown. **c**. Time course analysis of TCR/CD3 downregulation in control or IFT20-KD cells following receptor engagement with anti-CD3 mAb (n=3).

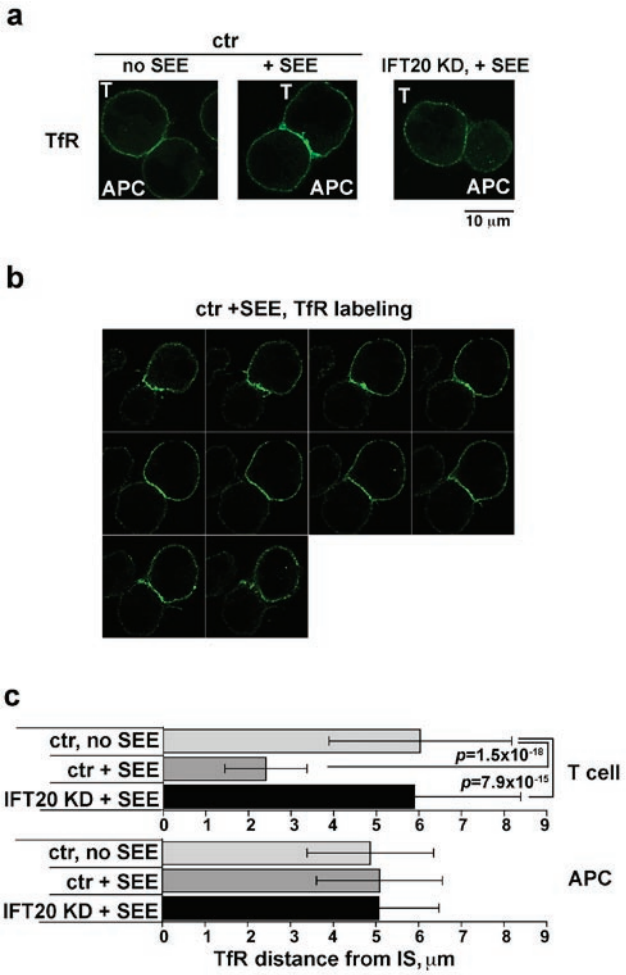

Figure S5 a. Immunofluorescence analysis of TfR localization in conjugates of control/IFT20-KD Jurkat cells and APC, in the presence or absence of SEE. Before conjugate formation, Raji cells were stained with CTB for identification. Cells were fixed in non-permeabilizing conditions. Median confocal sections are shown. **b**. Z-stack of a SEE-specific Jurkat/Raji conjugate fixed in non-permeabilizing conditions and immunostained with anti-TfR antibodies. **c**. Histograms showing the mean distance±SD of the central point of the TfR compartment from the T-cell/APC contact site (μm) on the T-cell side (top) or the APC side (bottom) of each conjugate. The measurements, which highlight the TfR polarization specifically on the T-cell side of the T-cell:APC contact site in antigen-specific conjugates of control Jurkat cells (but not IFT20-KD cells), were taken on conjugates from at least 3 independent experiments (n=50 conjugates). Error bars, SD.

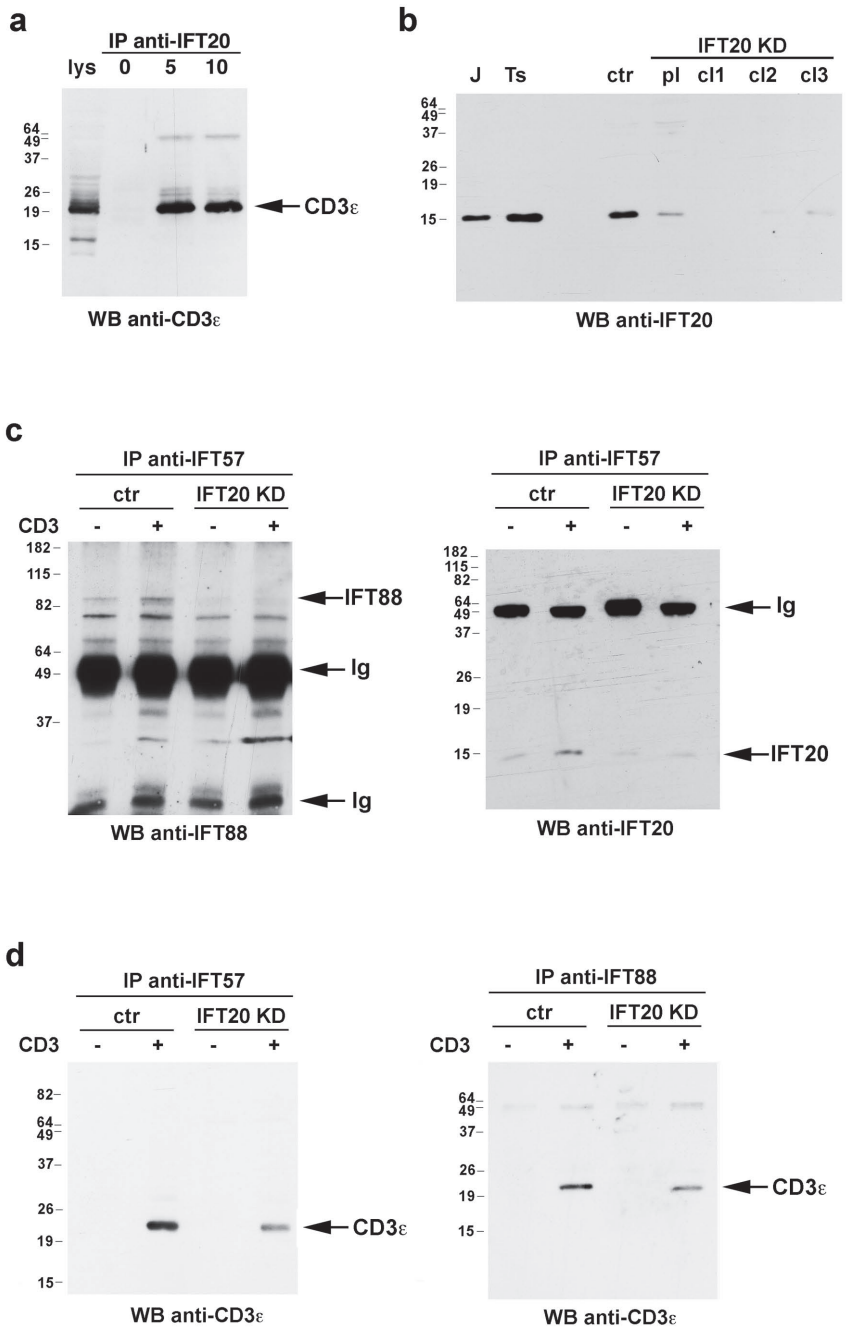

Figure S6 Full scans of key immunoblots. **a.** Full scan of immunoblot with anti-CD3ε antibodies of IFT20-specific immunoprecipitates from lysates of Jurkat cells stimulated with anti-CD3 mAb (shown in Fig.2c). **b**. Full scan of immunoblot of IFT20 in lysates of Jurkat cells, a Jurkat line transfected with empty vector (ctr), and three Jurkat clones (cl1-3) transfected with constructs encoding IFT20-specific siRNA (KD) (shown in Fig.2d). Ts, mouse testis lysate (positive control). **c**. Immunoblot analysis with anti-IFT88 (left) and anti-IFT20 (right) antibodies of anti-IFT57 specific immunoprecipitates from lysates of Jurkat cells either unstimulated or stimulated with anti-CD3 mAb for 10 min (shown in Fig.4b). Rabbit antibodies were used both for immunoprecipitation and for immunoblotting, accounting for the additional bands. **d**. Immunoblot analysis with anti-CD3ε antibodies of anti-IFT57 (left) or anti-IFT88 (right) specific immunoprecipitates from lysates of Jurkat cells either unstimulated or stimulated with anti-CD3 mAb for 10 min (shown in Fig.4b).

Supplementary Movie legends

Movie 1 Animation of the 3D reconstruction of IFT20 (red)/ GM130 (green) colocalization shown in figure 1c.

Movie 2 Animation of the 3D reconstruction of IFT20 (red)/ TGN46 (green) colocalization shown in figure 1c.

Movie 3 Animation of the 3D reconstruction of IFT20 (red)/ TfR (green) colocalization shown in figure 1c.

Movie 4. Animation of the 3D reconstruction of IFT20 (red)/ EEA1 (green) colocalization shown in figure 1c.

Movie 5 Animation of the 3D reconstruction of IFT20 (red)/ LAMP–1 (green) colocalization shown in figure 1c.

Movie 6 Animation of the 3D reconstruction of IFT20 (red)/γ-tubulin (green) colocalization shown in figure 1c.

Movie 7 Animation of the 3D reconstruction of IFT20 (red)/ IFT57 (green) colocalization shown in figure 4c.